Chapter 6
Continuous Modelling of Fracture in Plain Concrete under Cyclic Loading

Abstract. The enhanced coupled elasto-plastic damage models with non-local softening proposed by Pamin and de Borst (1999) (called model '1'), by Carol et al. (2001) and by Hansen and Willam (2001) (called model '2'), by Meschke et al. (1998) (called model '3') and Marzec and Tejchman (2009, 2010, 2011) (called model '4') described in detail in Chapter 3.2 were used in FE calculations. Quasi-static FE results were compared with corresponding laboratory tests on concrete specimens: dog-bone shaped specimen under monotonic uniaxial tension (van Vliet and van Mier 2000) and notched beams under cyclic loading (Hordijk 1991, Perdikaris and Romeo 1995).

Initial Results for Monotonic Uniaxial Tension

In the first step, the numerical calculations were carried out for concrete specimens under monotonic uniaxial tension. The main purpose was to check the effectiveness of a different non-local techniques used for each model. The experimental data presented by van Vliet and van Mier (2000) served as the reference data. In the experiments, a size effect in concrete with two-dimensional dog-bone shaped concrete specimens under quasi-static uniaxial tension (Fig. 6.1) was investigated. The five different specimen types (from 'A' to 'E') were used. Their height varied from 75 mm up to 2400 mm. In the numerical calculations, three different specimen sizes were considered only, namely: 'A', 'B' and 'C' (Tab. 6.1) with the height varying between 75 mm and 300 mm. The deformation was induced by imposing a vertical displacement at the node at the top part of the specimen. The number of triangular finite elements (with linear shape functions) was equal to 246, 1018 and 4102 for the specimen 'A', 'B' and 'C', respectively (with characteristic length l_c=5 mm). The modulus of elasticity was E=49.0 GPa and the Poisson's ratio was ν=0.2.

In the coupled model '1' by Pamin and de Borst (1999) (Chapter 3.2), the von Mises yield criterion with linear hardening was assumed in a plastic region (with the yield stress $\sigma_{yl}^{\ 0}$=2.6 MPa and linear hardening modulus $H_p=E/2$). In a damage regime, the following material parameters were assumed: $\kappa_0=7.9\times10^{-5}$, α=0.91, β=350 and k=10. The damage formulation was based on the total strain $\tilde{\varepsilon}\left(\varepsilon_{ij}\right)$.

J. Tejchman, J. Bobiński: Continuous & Discontinuous Modelling of Fracture, SSGG, pp. 163–182.
springerlink.com

In the coupled model '2' by Carol et al. (2001) and by Hansen and Willam (2001) (Chapter 3.2), the following parameters: E_{pt}=45 GPa, n_t=0.13 and f_t=2.54 MPa were assumed to describe the resistance function by Eq. 3.77. In turn the following parameters were chosen in the coupled model '3' by Meschke et al. (1998) (Chapter 3.2): f_t=2.85 MPa, κ_0=3.0×10^{-3} and β=0.15. For the coupled model '4' by Marzec and Tejchman (2010) (Chapter 3.2), the Rankine yield criterion with the yield stress σ^0_y=2.5 MPa was assumed in plasticity. A linear hardening parameter (H_p=E/2) was chosen. In a damage regime, the following material parameters were taken: κ_0=9×10^{-5}, α=0.95 and β=230. The damage formulation was based on the total strains according to Eq. 3.84. The stiffness reduction factors were a_t=1 and a_c=1.

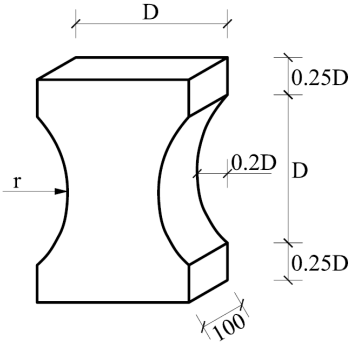

Fig. 6.1 Geometry of dog-bone shaped specimen (Vliet and van Mier 2000)

Table 6.1 Dimensions of dog-bone shaped specimens under uniaxial tension of Fig. 6.1 (van Vliet and van Mier 2000)

Specimen type (Fig. 6.1)	'A'	'B'	'C'
D [mm]	50	100	200
r [mm]	36.25	72.50	145

Figure 6.2 shows the calculated localized zone with four coupled models in the specimen A, B and C of Tab. 6.1. In turn, the calculated load-displacement diagrams for the concrete specimen 'B' of Tab. 6.1 with 4 coupled models compared to the experiment are demonstrated in Fig. 6.3. A satisfactory agreement with the experiment was obtained.

The calculated width of a localized zone is 2.2÷2.3 cm (4-5)×l_c (model '1' and '4'), 2.7 cm (5-6)×l_c (model '2') and 1.7 cm (3-4)×l_c (model '3'). The calculated evolution of the vertical force at the top is almost the same for each formulation and close to the experimental data.

Figure 6.4 presents a comparison of calculated and experimental values of the nominal strength σ_N versus the specimen size D (σ_N was calculated by dividing the

ultimate vertical force at the top by the smallest specimen cross-section equal to 0.6 bD, b – specimen thickness, D – specimen width of Fig. 6.1. The numerical results were compared with the corresponding experimental mean values (and standard deviations).

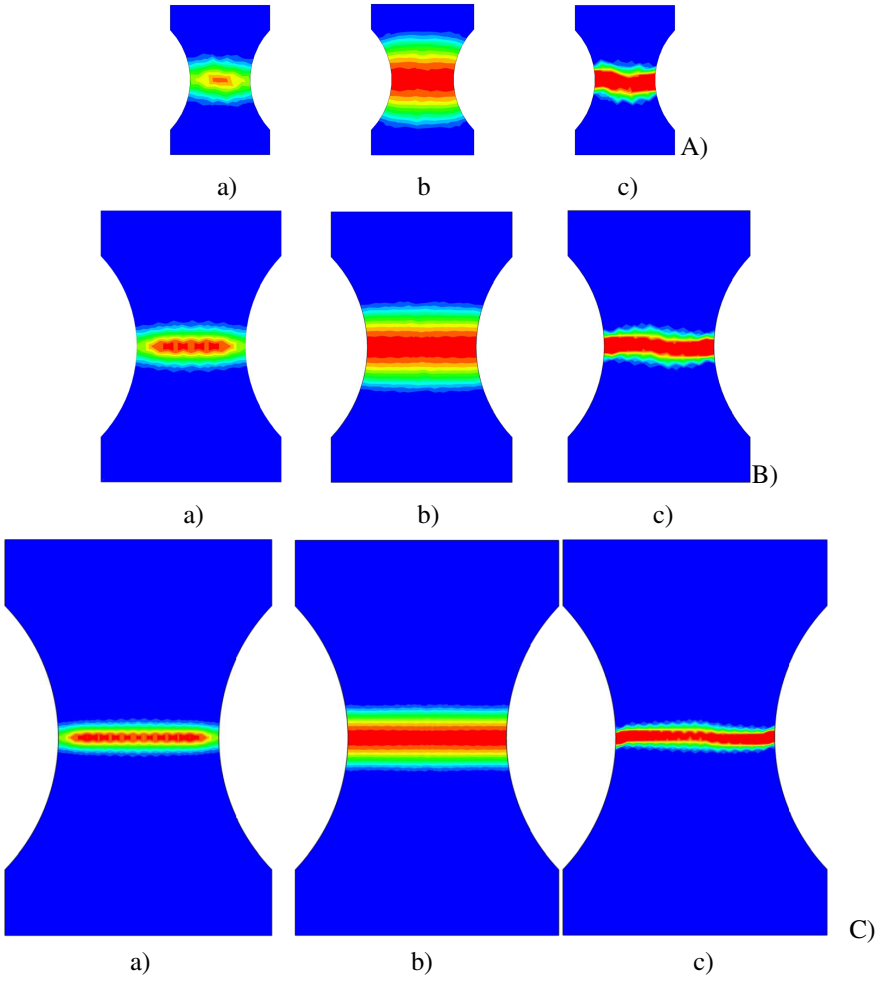

Fig. 6.2 Calculated contours of localized zones (for u=100 μm) with different enhanced coupled models: a) model '1' and '4', b) model '2' and c) model '3' for specimen sizes of Tab. 6.2: A) type A, B) type B and C) type C (Vliet and van Mier 2000) (specimens are not scaled)

Figure 6.5 shows the effect of a different resistance function (Eqs. 3.72, 3.76 and 3.77) in the coupled model '2' on results in a post-peak regime. The function of Eq. 3.72 gives limited possibilities to control the material behaviour in a softening regime (Fig. 6.5a), since a significant change of g_f/r_o slightly influences

the load-displacement curve. The proposition in Eq. 3.36 describes a wider range of the post-peak behaviour with the same amount of parameters as the previous function (Fig. 6.5b). The third resistance function of Eq. 3.77 can the best control the rate of softening and the shape of the function in the post-peak regime with the help of one additional parameter (Fig. 6.5c).

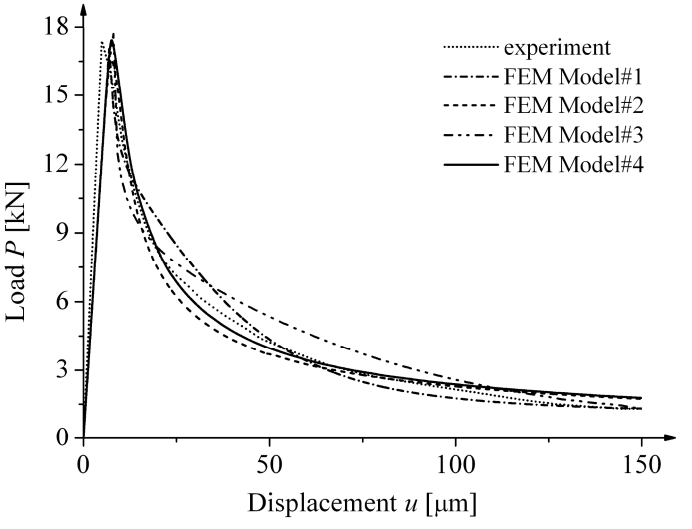

Fig. 6.3 Calculated load-displacement diagrams for four coupled elasto-plastic-damage models as compared with experimental data for specimen 'B' (Vliet and van Mier 2000)

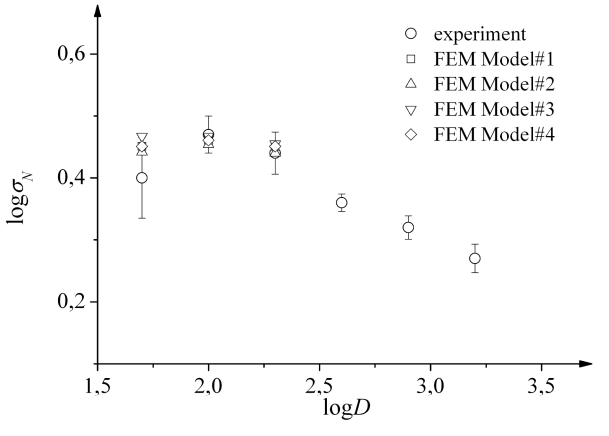

Fig. 6.4 Comparison between calculated and experimental values of nominal strength σ_N versus specimen size D of Fig. 6.1 for dog-bone shaped specimens (Vliet and van Mier 2000)

The experimental size effect on strength was well reflected in numerical calculations except the smallest specimen 'A' wherein a strong boundary effect took place in the experiment (the coarseness of the applied concrete mixture was simple too large in relation to the specimen dimensions, Vorechovsky 2007).

FE Results for Four-point Cyclic Bending of Notched Concrete Beams

The comparative numerical plane strain simulations were performed with a concrete notched beam under four-point cycling bending subjected to tensile failure (Hordijk 1991) (Fig. 6.6). The length of the beam was 0.5 m and the height 0.1 m. The deformation was induced by imposing a vertical displacement at two nodes at the top of the beam. In the calculations, the modulus of elasticity was E=40 GPa, Poisson ratio ν=0.2 and characteristic length l_c=5 mm. The tensile strength from experiments was varied between f_t=2.49 MPa and f_t=4.49 MPa. The calculations were performed with 7634 triangular finite elements. The size of elements was not greater than (2-3)×l_c to obtain objective FE results (Bobiński and Tejchman 2004, Marzec et al. 2007). The force-displacement diagrams P=f(u) are shown in Fig. 6.7. In turn, Fig. 6.8 presents the calculated contours of a localized zone above the notch. The evolution of non-local parameters: equivalent strain measure (model '1' and '4'), pseudo-log damage variable (model '2') and softening parameter (model '3') is demonstrated in Fig. 6.9.

For the first enhanced coupled model (model '1') with one surface in hardening plasticity, the von Mises criterion with the yield stress σ_{yt}^0=6.5 MPa (total strains) and σ_{yt}^0=5.9 MPa (elastic strains) was assumed with a linear hardening parameter (H_p=E/2). Since, an elasto-plastic model is not directly responsible for the evolution of the failure mechanism, the von Mises criterion was chosen for concrete in elasto-plasticity for the sake of simplicity (the application of the criterion by Drucker-Prager does not affect FE results). The following material constants were used: κ_0=9.5×10^{-5}, α=0.92 and β=140 with the total strains $\tilde{\varepsilon}\left(\varepsilon_{ij}\right)$, and κ_0=8.6×10^{-5}, α=0.92 and β=170 with the elastic strains $\tilde{\varepsilon}\left(\varepsilon_{ij}^e\right)$. The parameter set is different in both cases due to a varying coupling between plasticity and damage (via elastic or total strains).

Figure 6.7a shows the calculated load-displacement curves with a coupled elasto-plastic damage model using total strains. The load reversals exhibit a gradual decrease of the elastic stiffness, however calculated stiffness degradation is overestimate, especially for high values of κ. The calculated vertical force is close to experiment. The slope of the load-displacement curve is realistically reflected. The width of a localized zone above the notch in the beam is about 2.4 cm (4.8×l_c) (Fig. 6.9a).

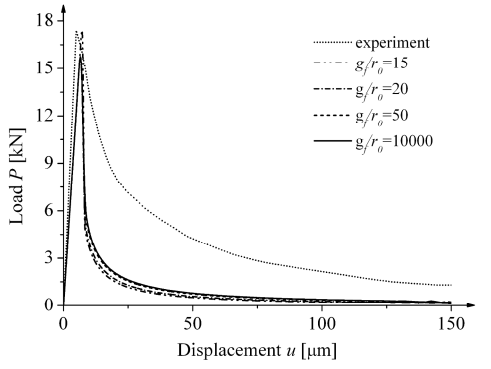

a)

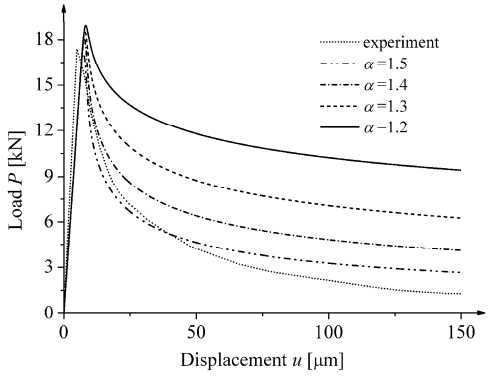

b)

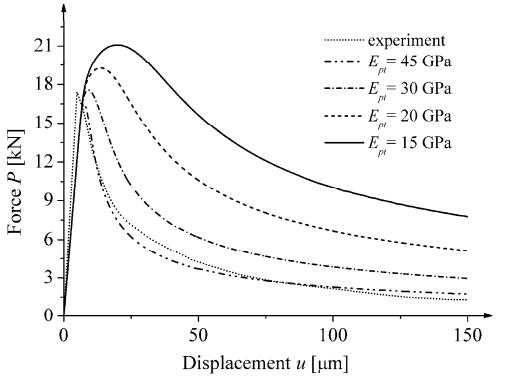

c)

Fig. 6.5 Calculated load-displacement curves with resistance functions: a) of Eq. 3.72 for different ratios g_f/r_0, b) of Eq. 3.76 for different parameter α and c) of Eq. 3.77 for different parameters E_{pt} and n_t compared with experimental data for specimen 'B' (Vliet and van Mier 2000)

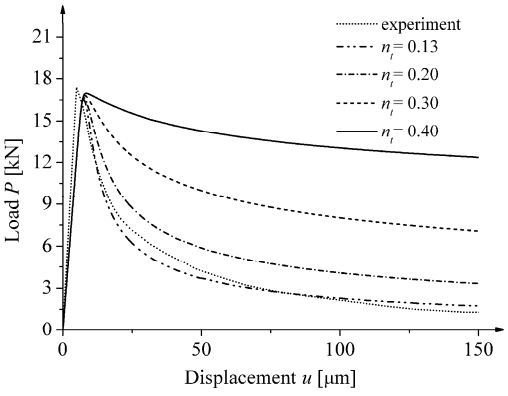

c)

Fig. 6.5 (*continued*)

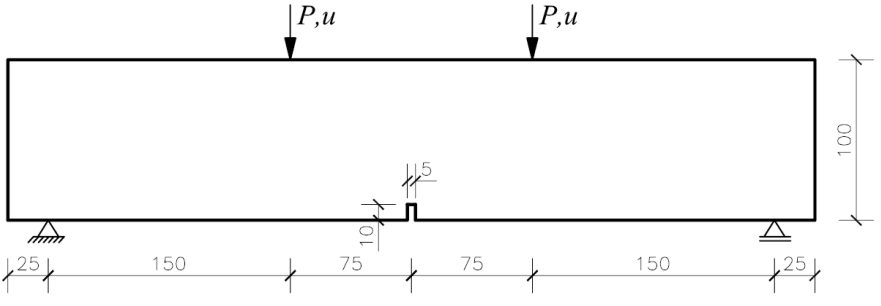

Fig. 6.6 Geometry and boundary conditions of a notched beam under four-point bending (Hordijk 1991)

Using the second enhanced coupled model, the resistance function by Nguyen (2005) was assumed with E_{pt}=37 GPa, n_t=0.175, f_t=2.85 MPa and m=1.2. The numerical results agree well with the experimental data only in the case of the ultimate vertical force and softening slope in the post-peak regime (Fig. 6.7b). The calculated stiffness degradation is significantly too high than in the experiment. As a consequence, the width of a localized zone increases up to 3.2 cm (6.4×l_c) (Fig. 6.9b). The similar results are obtained with the resistance function by Eq. 3.76 (Marzec 2009).

In the third enhanced coupled model, the calculated ultimate vertical force (with the parameters: f_t=2.85 MPa, κ_0=1.85×10^{-3}, γ=0.2 and m=2) again very similar as compared with the experimental value (Fig. 6.7c). Also the softening behaviour is realistically reflected. The slope of the experimental and numerical

curve is almost the same. The calculated stiffness degradation exhibits a proper gradual decrease and it is close to experiment. The width of the localized zone above the notch is 1.4 cm ($2.8 \times l_c$) (Fig. 6.9c).

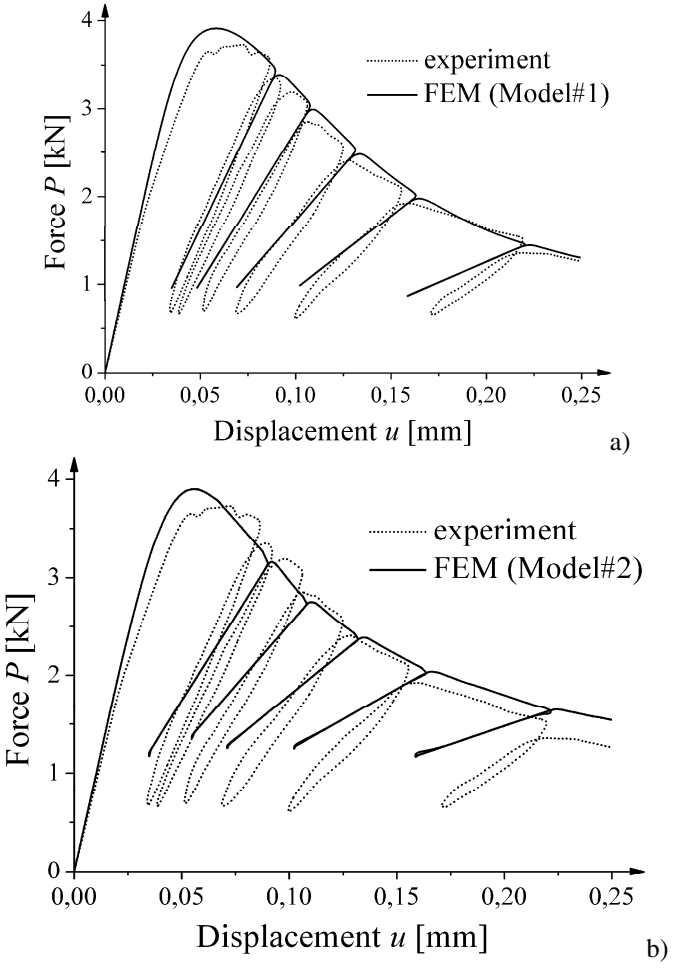

Fig. 6.7 Experimental and calculated force-displacement curves using 4 different coupled elasto-plastic-damage models with non-local softening during quasi-static four-point cyclic bending under tensile failure (Hordijk 1991): a) model '1' (damage based on total strains), b) model '2', c) model '3' and d) model '4' (damage based on elastic strains) (Marzec and Tejchman 2009, 2010)

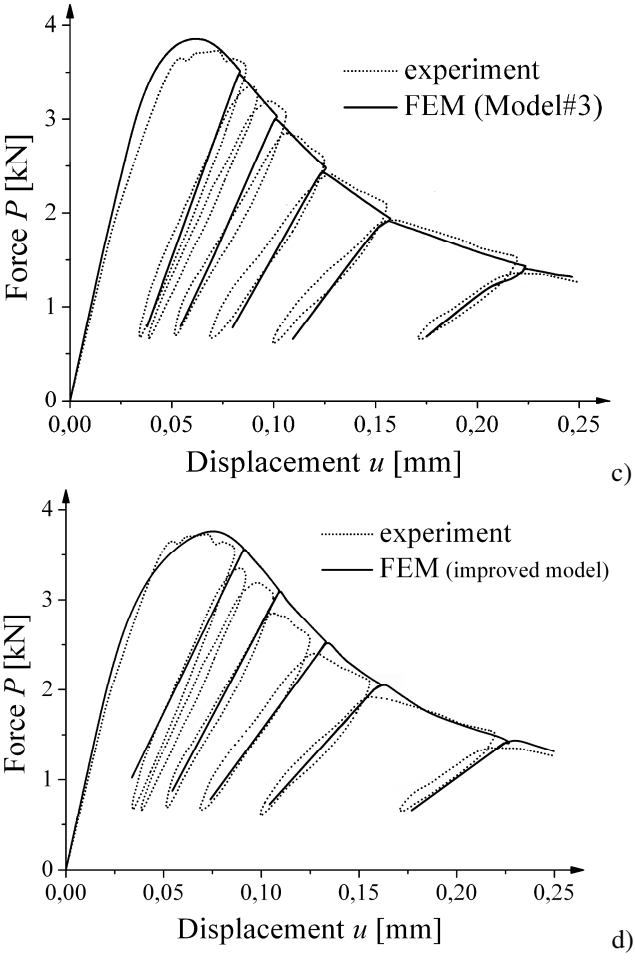

Fig. 6.7 (*continued*)

In the fourth enhanced model, the constants σ_{yt}^{0}=6.5 MPa, H_p=E/2, κ_0=4.3×10^{-5}, β=650, α=0.90, η_1=1.2, η_2=0.15, δ=450, a_t=0 and a_c=1 were used (damage was based on elastic strains). The calculated force-displacement curve exhibits good agreement with experimental outcomes (Fig. 6.7d). The bearing capacity of the beam is very well captured. The post-peak behaviour is close to experiment, however the softening slope is slightly worst reflected as in the model '3'. In turn a calculated stiffness decrease is almost the same as in the experiment. Thus, an evident improvement as compared to the model '1' with respect to the magnitude of the stiffness reduction was achieved. The calculated contours of a non-local variable describing the shape of a localized zone are similar as in the model '1' (Fig. 6.8d). The results of Figs. 6.8 and 6.9 demonstrate that the shape of a localized

zone above the notch is different due to the material stiffness in a softening regime induced by the material formulation. The shape of a localized zone in the models '1' and '4' is the same due to a similar model formulation, and is typical for other solutions within damage mechanics (e.g. Peerlings 1999, Pamin and de Borst 1999).

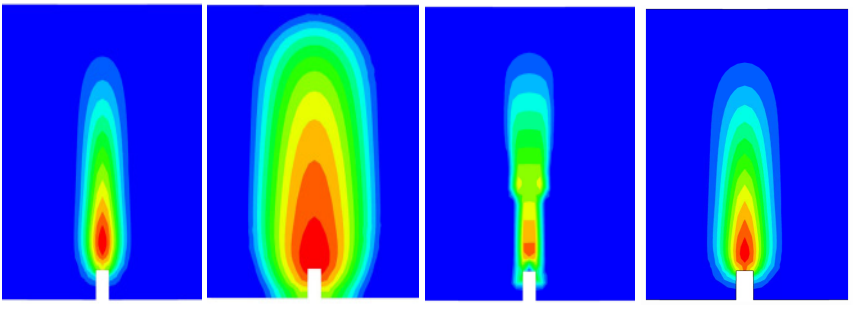

Fig. 6.8 Calculated contours of localized zone near notch in a beam under four-point bending with 4 different coupled elasto-plastic-damage models with non-local softening during four-point bending: a) model '1', b) model '2', c) model '3' and d) model '4' (at deflection u=0.15 mm) (Marzec and Tejchman 2010)

Summarized, the coupled models '1', '3' and '4' are capable to satisfactorily capture the cyclic concrete behaviour under tensile failure.

FE results for three-point cyclic bending of notched concrete beams

In order to check the capability of the improved coupled model '4' to simulate a deterministic size effect observed experimentally in brittle materials (van Vliet and van Mier, 2000), the FE-calculations were performed in addition with concrete notched beams under three-point cycling loading (Fig. 6.10 Tab. 6.2) (Perdikaris and Romeo 1995). The number of triangular finite elements was equal to 2292, 5213 and 9211 for a small-, medium- and large-size beam, respectively. The size of elements was again not greater than $3\times l_c$. The deformation was induced by imposing a vertical displacement at the mid-node at the beam top. The modulus of elasticity was E=45.6 GPa and the Poisson ratio was ν=0.2 and. To match the numerical results with the experimental ones, the same material constants for all three beams were chosen: σ^0_y=6.5 MPa, $H_p=E/2$, $\kappa_0=9.0\times10^{-5}$, β=1550, α=0.99, η_1=1.2, η_2=0.15, δ=950, a_t=0 and a_c=1 and l_c=5 mm (equivalent strain measure based on elastic strains). As compared to FE calculations on four-point cyclic bending, the same constants σ_y, H_p, η_1, η_2, a_t and a_c were assumed.

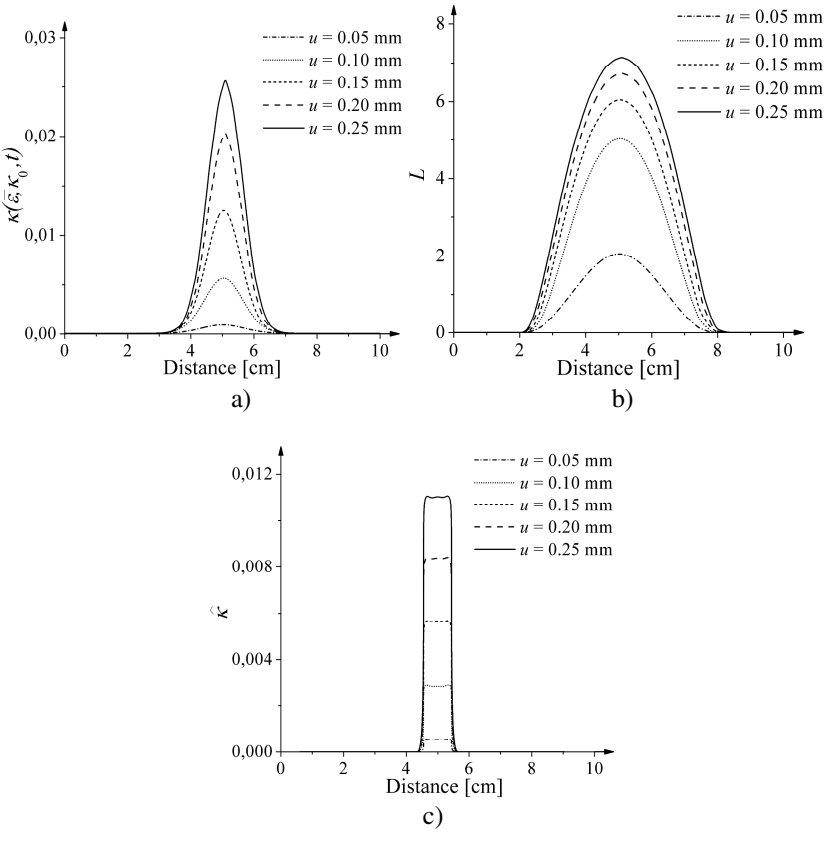

Fig. 6.9 Evolution of non-local parameter above notch in beam under four-point bending with 4 different coupled elasto-plastic-damage models with non-local softening: a) model '1', b) model '2' and c) model '3' (at deflection u=0.15 mm) (Marzec and Tejchman 2009)

Figures 6.11a and 6.11b demonstrate the calculated force-displacement diagrams for a small- and large-size beam compared with the experimental data. The stiffness degradation is again realistically captured by the model. The calculated ultimate force as compared to experiments is higher by 10-15%. To obtain a better agreement between ultimate forces and calculated stiffness, the material constant should be better calibrated (in particular κ_0 and parameters controlling the damage evolution β, δ and η_2).

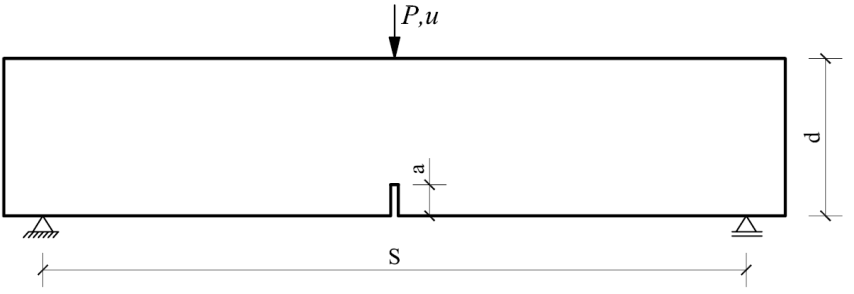

Fig. 6.10 Geometry and boundary conditions of a notched beam under three-point cyclic bending (Perdikaris and Romeo 1995)

Table 6.2 Beam dimensions in cyclic tests by Perdikaris and Romeo (1995)

Beam Size	Depth *d*	Width *b*	Span *S*	Notch *a*
	[mm]	[mm]	[mm]	[mm]
Small	64	127	254	20
Medium	128	127	508	39
Large	254	127	1016	78

Next, the calculated results of a deterministic size effect with respect to the ultimate vertical force were confronted with the size effect law by Bažant (Eq. 5.5) for notched beams (Bažant and Planas 1998, Bažant 2003). The FE results show good agreement with the experimental data (Fig. 6.12).

First, simple cyclic uniaxial element tests were numerically performed to show the behaviour of the model '4' (with 4-node quadrilateral elements). Figure 6.13 shows the load-displacement diagrams under cyclic uniaxial tension and cyclic uniaxial compression for different influential material constants β, δ, η_2 and κ_0 (which were independently changed). The effect of the constant α (α=0.7-0.99) and η_1 (η_1=1.0-1.2) was negligible. The modulus of elasticity was E=40 GPa and the Poisson ratio was ν=0.18. In tension, the constants σ^0_y=4.0 MPa and $H_p=E/2$ (Rankine criterion), and in compression σ^0_y=40 MPa, $H_p=E/2$, ϕ=20º and ψ=10º (Drucker-Prager criterion) were chosen. The equivalent strain measure was based on total strains. The material constants varied in the following ranges: β=200-1100, δ=200-900, η_2=0.15-0.45 and κ_0=(15-25)×10^{-5} (with α=0.95, η_1=1.2, a_t=0.0 and a_c=1.0). The force-displacement results indicate that the effect of κ_0 is significant in tension and the effect of δ, η_2 and κ_0 in compression. The parameter κ_0 is responsible for a peak location and a simultaneous activation of a plastic and damage criterion. The parameters β, δ and η_2 affect a model response in softening

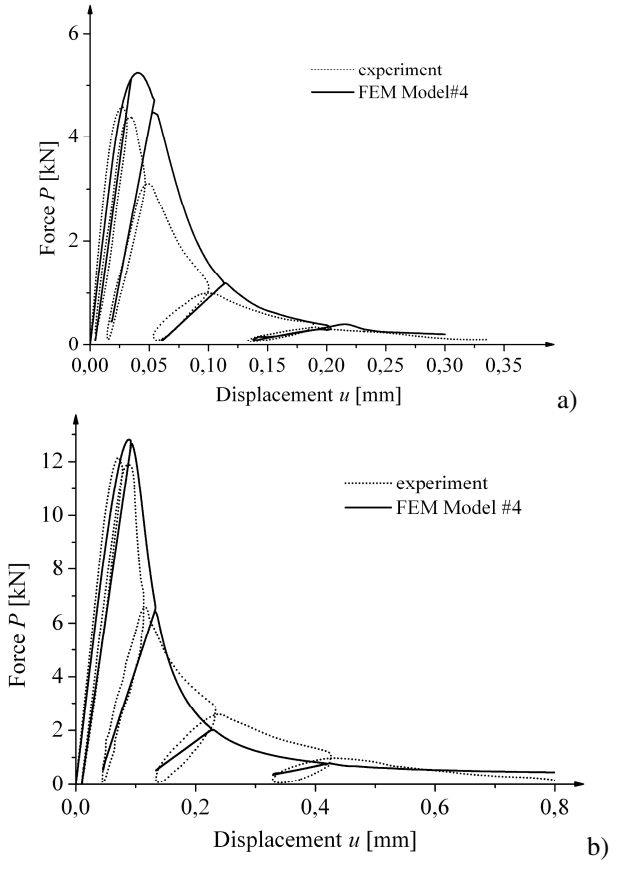

Fig. 6.11 Experimental (Perdikaris and Romeo 1995) and calculated load-displacement curves with enhanced coupled model '4' with damage based on elastic strains (quasi-static cyclic three-point bending): a) small-size beam, b) large-size beam (a_t=0.0 and a_c=1.0) (Marzec and Tejchman 2010)

during tension and compression, and the parameter η_2 influences a hardening curve in compression. The effect of two other parameters (α and η_1) describing the stress-strain curve at the residual state is negligible.

Cyclic behaviour of concrete under compression and tension

Next, a simple cyclic tension-compression-tension element test was calculated (Fig. 6.14) ($\sigma_{yt}^{\ 0}$=4 MPa, $\sigma_{yc}^{\ 0}$=40 MPa, $H_p=E/2$, ϕ=20º, ψ=10º, β=550, δ=950, $\kappa_0=8.5\times10^{-5}$, α=0.95, η_1=1.2, η_2=0.15, a_t=0.0 and a_c=1.0). The results show obviously the different stiffness degradation during compression and tension (that is stronger in tension). A recovery of the compressive stiffness upon crack closure and un-recovery of the tensile stiffness as the load changes between tension and compression is satisfactorily reflected. The evident difference between a pure

damage model (without plastic strains) and coupled one (with plastic strains) during one uniaxial load cycle is demonstrated in Fig. 6.15.

The effect of the damage scale factors a_t and a_c on the load-displacement diagram under tension-compression-tension is described in Fig. 6.16 by assuming a_t=0.2 and a_c=0.8. This change of both factors is stronger in compression.

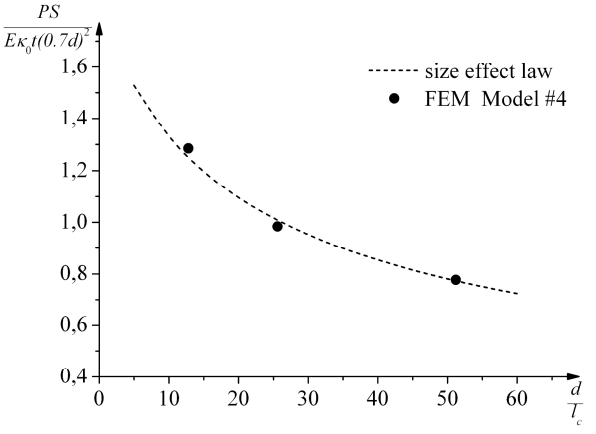

Fig. 6.12 Calculated deterministic size effect for concrete notched beams subjected to quasi-static cyclic three-point bending (using coupled model '4') as compared with size effect law by Bažant (Eq. 5.5) (Bažant 2003) (t – beam thickness, d - beam height, S – beam span)

Finally, Fig. 6.17 demonstrates the 2D FE results with the model '4' for a concrete specimen subjected to uniaxial cyclic compression by taking strain localization into account. All nodes at the lower edge of a rectangular specimen were fixed in a vertical direction. The size of the specimen was arbitrarily chosen: 15 cm (height) and 5 cm (width). To preserve the stability of the specimen, the node in the middle of the lower edge was kept fixed. The deformations were initiated through constant vertical displacement increments prescribed to nodes along the upper edge of the specimen. The lower and upper edges were smooth. The number of triangular finite elements was 896 (the size of elements was not greater than $3\times l_c$). The material constants were: E=30 GPa, ν=0.18, $\sigma_{yc}^{\ 0}$=20 MPa, ϕ=25º, ψ=10º, η_1=1.2, η_2=0.7, δ=800, l_c=5 mm, a_t=0.0 and a_c=1.0. To induce strain localization, a weak element was inserted in the middle of height, on edge of the specimen. Due to the lack of the initial experimental data, the calculated stress-strain curve was qualitatively compared with the experimental one by Karsan and Jirsa (1969) (Fig. 6.17).

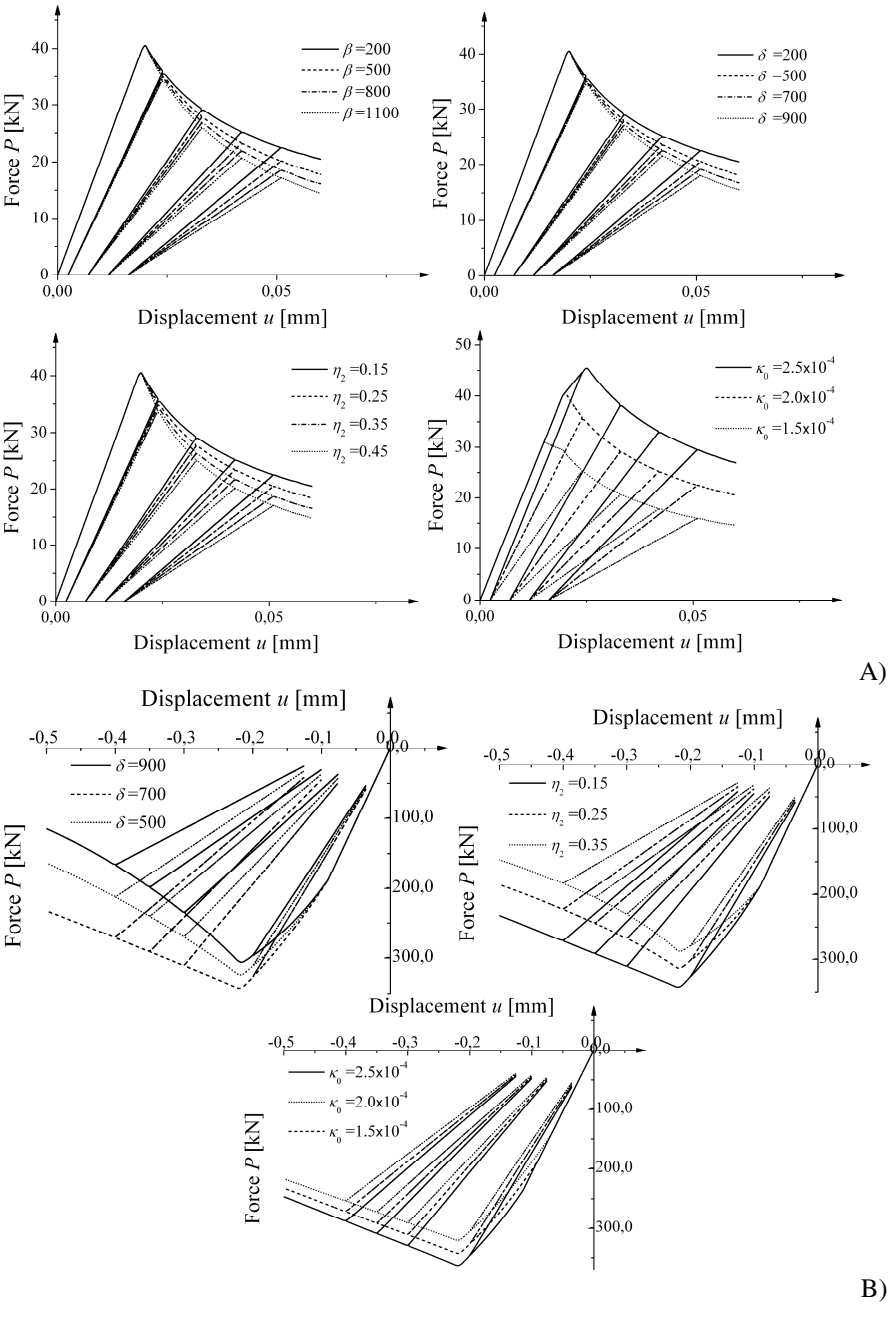

Fig. 6.13 Effect of different material constants on uniaxial response of coupled elasto-plastic-damage model '4' for concrete under: A) cyclic uniaxial tension and B) cyclic uniaxial compression (with damage scale factors a_t=0.0 and a_c=1.0) (Marzec and Tejchman 2010)

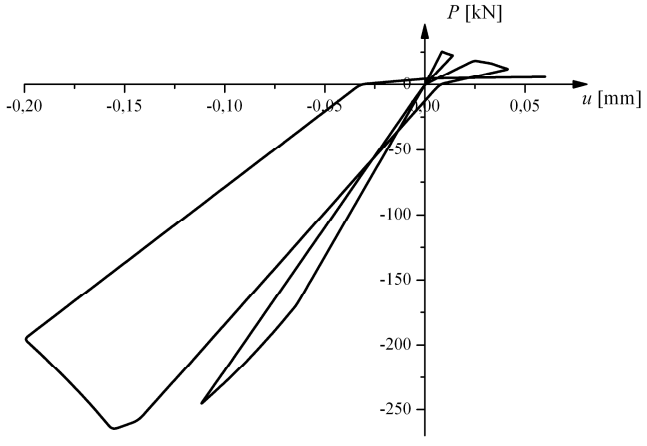

Fig. 6.14 Calculated load-displacement curve with coupled model '4' (with damage scale factors a_t=0.0 and a_c=1.0) during uniaxial tension-compression-tension (Marzec and Tejchman 2010)

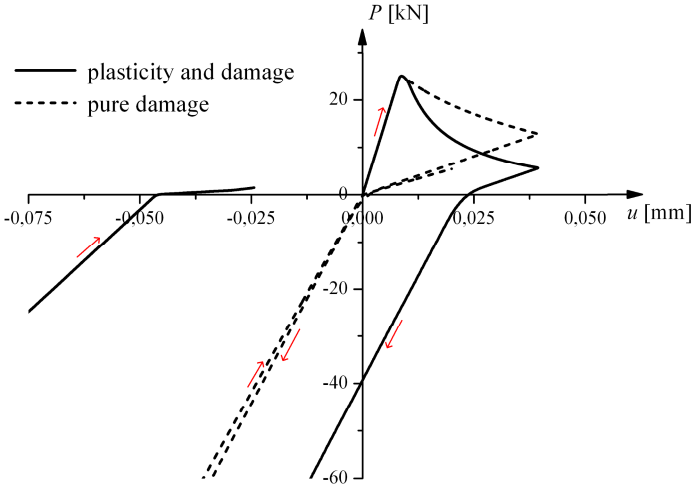

Fig. 6.15 Calculated load-displacement curves with coupled model '4' during uniaxial tension-compression-tension with and without plastic strains (Marzec and Tejchman 2010)

The calculated stress-strain curve (Figs. 6.17c and 6.17d) is qualitatively the same as in a cyclic compressive test by Karsan and Jirsa (1969) (Figs. 6.17c and 6.17e) with respect to material softening and stiffness degradation. The calculated thickness of a localized zone is 3.4 cm ($6.8 \times l_c$) and the inclination to the horizontal is about 45^o (Fig. 6.17a and 6.17b). These results are very similar to those within elasto-plastic calculations (Bobiński and Tejchman 2004). The shear

zone inclination is significantly higher (and more realistic) than that obtained with a simple non-local isotropic damage model (Simone et al. 2002), which was smaller than 35^o-40^o.

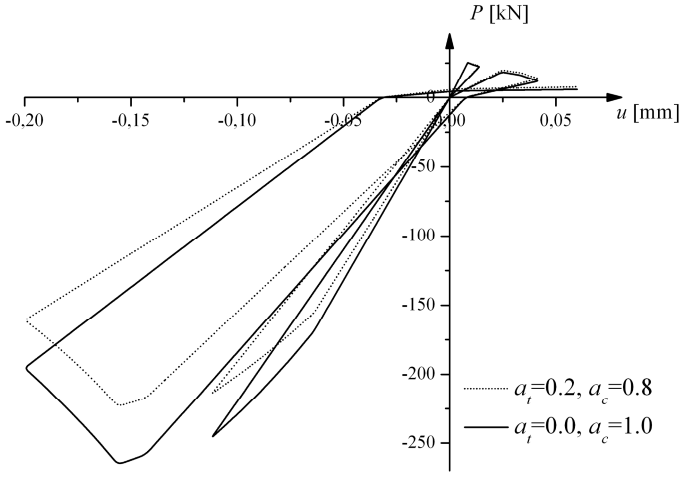

Fig. 6.16 Uniaxial response of coupled elasto-plastic-damage model '4' for concrete under tension-compression-tension for different damage scale factors a_t and a_c (Marzec and Tejchman 2010)

The following conclusions can be derived:

- The FE calculations show that the coupled elasto-plastic damage models used enhanced by a characteristic length of micro-structure in a softening regime can properly reproduce the experimental load-displacement diagrams and strain localization in plain concrete notched beams under tensile loading during quasi-static cyclic bending. All models '1-4' properly capture material softening and the width of a localized zone. The models '1', '3' and '4' are also able to correctly describe the stiffness degradation. The drawback of the model '2' is the lack of possibility to simulate simultaneously both plastic deformation and stiffness degradation during cyclic loading. The model '3' has the smallest number of material constants to be calibrated. The coupled models '3' and '4' indicate the best agreement with cyclic bending experiments under tensile failure. In general, the models 1, 3 and 4 show similar results under tension. The shape and thickness of a localized zone above the notch in concrete beams under tension depends on the coupled formulation.
- A choice of a suitable local state variable for non-local averaging strongly depends on the model used. It should be carefully checked to avoid problems with non-sufficient regularization.

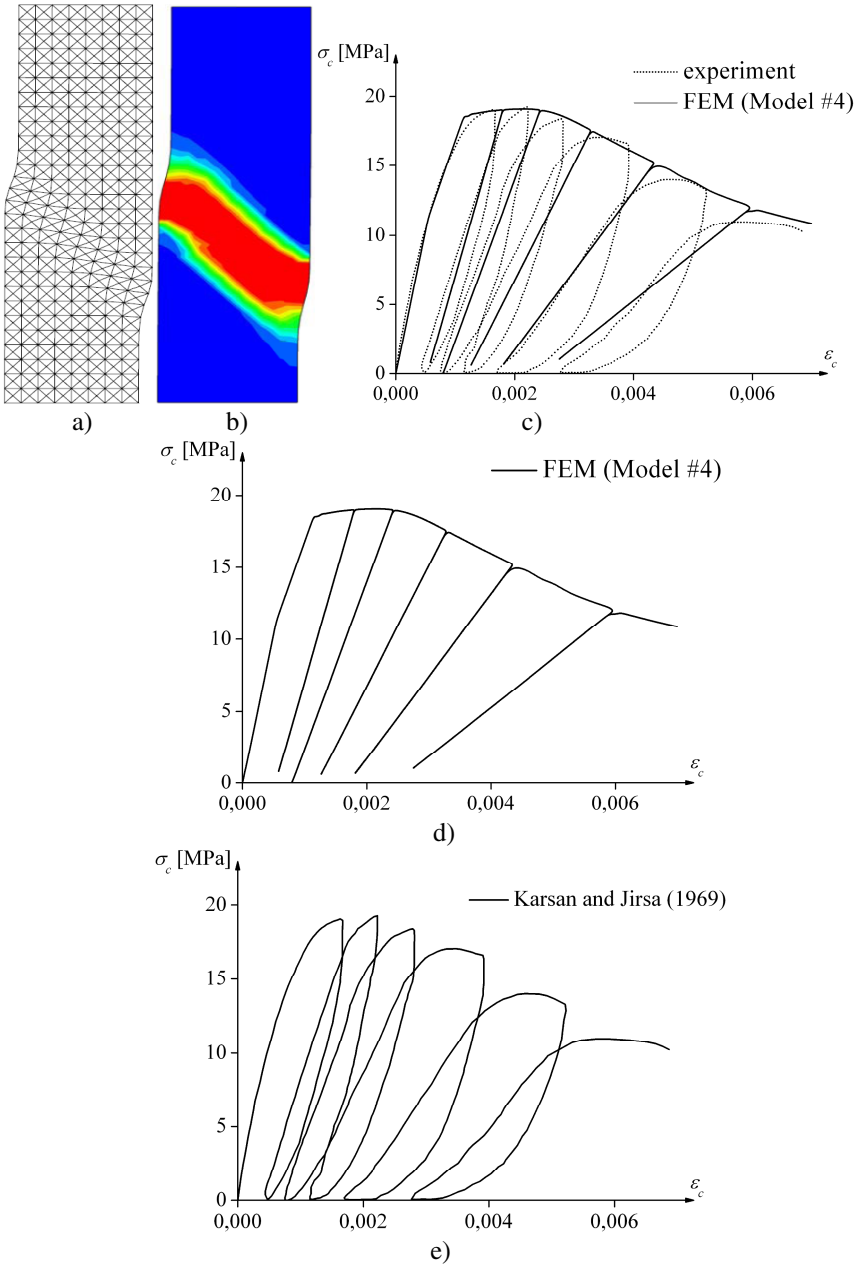

Fig. 6.17 Response of coupled elasto-plastic-damage model '4' for concrete specimen under uniaxial cyclic compression from FE calculations (with damage scale factors a_t=0.0 and a_c=1.0): a) deformed FE mesh, b) contours of calculated non-local parameter, c) calculated and experimental stress-strain curve by Karsan and Jirsa (1969), d) calculated stress-strain stress-strain curve, e) experimental stress-strain curve by Karsan and Jirsa (1969)

• The improved model '4' captures in addition plastic strains and stiffness degradation in both tension and compression, and stiffness recovery effect during cyclic loading by means of a strain equivalence hypothesis (thus the coupling between damage and plasticity is different than in ABAQUS 2004). It is able to properly describe strain localization under both tension and compression due to a presence of a characteristic length of micro-structure. Its drawback is no clear distinction between elastic, plastic and damage strain rates, and a relatively large number of material constants to be calibrated. Most of material constants may be calibrated independently with a monotonic uniaxial compression and tension (bending) test. Standard uniaxial cyclic tests are needed to calibrate damage scale factors.

References

ABAQUS, Theory Manual, Version 5.8, Hibbit. Karlsson & Sorensen Inc. (1998)

Bažant, Z.P., Planas, J.: Fracture and size effect in concrete and other quasibrittle materials. CRC Press LLC (1998)

Bažant, Z.P.: Scaling of Structural Strength. Hermes-Penton, London (2003)

Bobiński, J., Tejchman, J.: Numerical simulations of localization of deformation in quasi brittle materials within non-local softening plasticity. Computers and Concrete 1(4), 433–455 (2004)

Carol, I., Rizzi, E., Willam, K.: On the formulation of anisotropic elastic degradation. Int. J. of Solids and Structures 38(4), 491–518 (2001)

Hansen, N.R., Schreyer, H.L.: A thermodynamically consistent framework for theories of elastoplasticity coupled with damage. International Journal of Solids and Structures 31(3), 359–389 (1994)

Hansen, E., Willam, K.: A two-surface anisotropic damage-plasticity model for plane concrete. In: de Borst, R. (ed.) Procceedings Int. Conf. Fracture Mechanics of Concrete Materials, Paris, Balkema, pp. 549–556 (2001)

Hordijk, D.A.: Local approach to fatigue of concrete. PhD Thesis. Delft University of Technology (1991)

Karsan, D., Jirsa, J.O.: Behaviour of concrete under compressive loadings. Journal of the Structural Division (ASCE) 95(12), 2543–2563 (1969)

Marzec, I.: Application of coupled elasto-plastic-damage models with non-local softening to concrete cyclic behaviour. PhD Thesis, Gdańsk University of Technology (2009)

Marzec, I., Bobiński, J., Tejchman, J.: Simulations of crack spacing in reinforced concrete beams using elastic-plastic and damage with non-local softening. Computers and Concrete 4(5), 377–403 (2007)

Marzec, I., Tejchman, J.: Modeling of concrete behaviour under cyclic loading using different coupled elasto-plastic-damage models with non-local softening. In: Oñate, E., Owen, D.R.J. (eds.) X International Conference on Computational Plasticity-COMPLAS X, pp. 1–4. CIMNE, Barcelona (2009)

Marzec, I., Tejchman, J.: Application of enhanced elasto-plastic damage models to concrete under quasi-static and dynamic cyclic loading. In: Bicanic, N., de Borst, R., Mang, H., Meschke, G. (eds.) Modelling of Concrete Structures, pp. 529–536. Taylor and Francis Group, London (2010)

Marzec, I., Tejchman, J.: Application of coupled elasto-plastic-damage models with non-local softening to cyclic concrete behaviour. Archives of Mechanics (2011) (under review)

Meschke, G., Lackner, R., Mang, H.A.: An anisotropic elastoplastic-damage model for plain concrete. International Journal for Numerical Methods in Engineering 42(4), 702–727 (1998)

Nguyen, G.D.: A thermodynamic approach to constitutive modelling of concrete using damage mechanics and plasticity theory, PhD Thesis, Trinity College, University of Oxford (2005)

Pamin, J., de Borst, R.: Stiffness degradation in gradient-dependent coupled damage-plasticity. Archives of Mechanics 51(3-4), 419–446 (1999)

Peerlings, R.H.J.: Enhanced damage modeling for fracture and fatigue. PhD Thesis, TU Eindhoven, Eindhoven (1999)

Perdikaris, P.C., Romeo, A.: Size effect on fracture energy of concrete and stability issues in three-point bending fracture toughness testing. ACI Material Journal 92(5), 483–496 (1995)

Simone, A., Wells, G.N., Sluys, L.J.: Discontinuous modelling of crack propagation in a gradient enhanced continuum. In: Proc. of the Fifth World Congress on Computational Mechanics, WCCM V, Vienna (2002)

van Vliet, M.R.A., van Mier, J.G.M.: Experimental investigation of size effect in concrete and sandstone under uniaxial tension. Engineering Fracture Mechanics 65(2-3), 165–188 (2000)

Vorechovsky, M.: Interplay of size effects in concrete specimens under tension studied via computational stochastic fracture mechanics. International Journal of Solids and Structures 44(9), 2715–2731 (2007)